

# Kondo effect by controlled cleavage of a single molecule contact

R. Temirov and F.S. Tautz\*

*School of Engineering and Science, International University Bremen<sup>+</sup>, P.O. Box 750561, 28725 Bremen, Germany*

The Kondo effect in nanoelectronic devices has attracted attention because controllable model systems, ranging from single electron transistors<sup>1-4</sup>, carbon nanotubes<sup>5,6</sup> to single organo-metallic molecules<sup>7-9</sup>, allow systematic investigations of complex many-body effects in electronic structure and electron transport. Many intriguing variants of the Kondo effect have been discovered in this way<sup>10</sup>. Since the lead coupling is an important parameter in Kondo physics, a weakness of experiments to date, particularly on molecules and nanotubes, has been the lack of structural definition at the contacts between the metal leads and the Kondo centre. More generally, contact properties are in fact one of the unresolved challenges in the rapidly growing field of molecular electronics<sup>11,12</sup>. Here we present a single-molecule transport experiment with optimum control over contacts, carried out in an STM in a symmetric configuration, i.e. with a molecule between two chemical contacts. We start with a geometrically and spectroscopically well-characterized chemical bond between a  $\pi$ -conjugated molecule and a single crystalline metal surface<sup>13-18</sup> and vary this contact by a controllable and gradual structural modification, until the metal-molecule bond is cleaved. In this way, the molecular wire is tuned smoothly from the mixed-valence strong-coupling to the intermediate-coupling Kondo regime. This tuning is achieved by a gradual de-

---

\* Corresponding author (s.tautz@iu-bremen.de)

<sup>+</sup> Jacobs University Bremen as of spring 2007

**hybridisation of a molecular orbital from the metallic states due to mechanical stress. Apart from allowing a future *ab initio* analysis of Kondo physics in a single molecule, these experiments also suggest a new pathway to well-defined single molecule transport experiments in general.**

Our approach to single-molecule transport experiments is based on perfectly ordered, epitaxial layers of molecules on a single crystalline metal substrate. Such layers offer the advantage that molecules are adsorbed in well-defined adsorption sites; the electronic properties of the metal-molecule contact can therefore be characterized by a wide range of spectroscopic experiments.

Experiments have been carried out on the PTCDA (4,9,10-perylene-tetracarboxylic-dianhydrid) molecule (Fig. 1a). The epitaxial PTCDA/Ag(111) interface (cf. Fig. 2a) is a model organic/metal interface, for which a large number of integrating<sup>14,16</sup> and single molecule spectroscopies<sup>17,18</sup> as well as structural probes<sup>13,15,17</sup> have revealed a chemisorptive substrate-bonding of PTCDA through the  $\pi$ -electrons of its perylene core. Fig. 1a summarizes the most important properties of the PTCDA-Ag contact: The former LUMO of the molecule hybridises with metal states<sup>16,17</sup> (label i) and is pulled partially below the Fermi level<sup>14,16</sup>. In addition, there is a second interaction mechanism which involves bonds between the carboxylic oxygen atoms and the silver surface (label ii)<sup>15</sup>; the latter also leads to a buckling distortion of the adsorbed molecule<sup>15</sup>.

The second contact which is necessary for a transport experiment is established as a chemical bond between a defined atom of the surface-adsorbed PTCDA molecule and the STM tip (Fig. 1a). A first hint that it is indeed possible to establish a well-defined covalent contact between the STM tip and a PTCDA molecule comes from STM imaging experiments. In the constant current image Fig. 2b the conductance of the

junction rises abruptly by a factor of ten at periodic positions in the image, indicating a transient transition of the junction from tunnelling to contact and back within 1 Å diameter. This transition exhibits complete chemical specificity and occurs only at carboxylic oxygen atoms (marked red in Fig. 1a). Sometimes, as in Fig. 2b, only some of the carboxylic oxygens respond, but it must be remembered that in the herringbone layer they are not all structurally equivalent<sup>17</sup>. Also, under the present imaging conditions we have never observed an offset between the tunnelling image in Fig. 2b and the contact points, proving that electron tunnelling and “mechanical” contact formation occur through the same atom on the tip apex.

The contact formation can be investigated more systematically by placing the tip above a carboxylic oxygen atom and recording the conductance during a tip approach (Fig. 2c). Once the tip has reached the height of  $\sim 2.2$  Å above the carboxylic oxygen atom (see Methods for the determination of the absolute height), the conductance of the junction again jumps by a factor of approximately ten. Given the buckling of the molecule (Fig. 1a), it is easily conceivable that under the additional influence of the approaching tip the carboxylic oxygens may flip up to a new potential minimum a few tenths of an Angstrom above the plane of the molecule. Retracting the tip again, we observe in Fig. 2c hysteresis before the oxygen atom snaps back to its position close to the surface.

Characterizing the tip-molecule contact further we first note that contact formation proceeds independent of tip bias, i.e. the underlying inter-atomic force is field-independent (van der Waals or chemical); the size of the contact conductance (peaked around  $0.1 G_0$ , Fig. 2d) already suggests a chemical bond<sup>19</sup>. Second, by recording the distance at which the flip occurs, it is possible to resolve a clear 0.2 Å difference in the response of molecules of type A and type B (Fig. 2e). This observation in fact proves that the oxygen atoms flip up (Supplementary Information a). Third, once

formed the tip-molecule contact allows the reliable removal of PTCDA molecules from the surface, as the artificial vacancy structure in the inset of Fig. 2a demonstrates.

Fourth, it is possible to pass a current of in the microampere range through the contact, similar to other covalent contacts<sup>20,21</sup>. Fifth, the estimated contact distance of  $(2.9 \pm 0.8)$  Å (cf. Methods and Supplementary Information b for details) agrees reasonably well with covalent Ag-O distances in coordination compounds, e.g.  $(2.35 \pm 0.07)$  Å in ref. 22. All these observations prove that the tip-PTCDA contact is a covalent bond.

Concluding the discussion thus far, it is clear that a single PTCDA molecule can be joined between two covalent contacts. The contact to the substrate (hereafter called S-contact) is formed primarily by the extended  $\pi$ -electrons of the LUMO, while the contact to the tip (T-contact) proceeds via a single carboxylic oxygen atom. These two contacts are connected by the partially occupied (metallic) former LUMO of the molecule as the transport orbital (cf. Fig. 1a).

To study the electronic properties of this “molecular wire”, let us consider the approach and retraction curve in the inset of Fig. 3a, in which the initial conductance (at 2 mV bias) is plotted as a function of tip height above the molecular layer. Apparently, the T-contact does not break in this experiment, otherwise a behaviour as in Fig. 2c would be observed. During tip retraction, the conductance of the junction rises sharply and reaches a maximum of approx.  $0.2 G_0$  (also cf. green curve in Fig. 2d). This behaviour is observed regularly, as the collection of data in Fig. 3a shows. In experiments in which a molecule is removed from the surface, the conductance always exhibits the intermediate state with maximum conductance.

For a given molecule, the junction conductance is determined by the coupling constants  $\Gamma_S$  and  $\Gamma_T$  at the contacts<sup>11</sup> defined in Fig. 1b. Even for non-interacting electrons, a maximum junction conductance is expected for  $\Gamma$  of intermediate strength:

If  $\Gamma$  is too small, electron transfer across the contacts is inefficient, while a very large  $\Gamma$  hinders transport across the molecule by localising electrons too strongly in the contacts<sup>23</sup>. From the behaviour in Fig. 3a we thus conclude that the wire evolves from strong to intermediate lead coupling upon stretching  $\Gamma_S$  – or, in other words, the S-contact is cleaved gradually, as indicated schematically Fig. 1b. Here, we only consider  $\Gamma_S$  because the stronger T-contact will be less affected by the mechanical stress due to tip retraction. It must be noted, however, that the remarkable strength of the conductance increase when entering the intermediate coupling regime in Fig. 3a requires the presence of many-body correlations, as will be shown below.

Taking advantage of the unique possibility to study single molecule transport with a gradually tunable lead coupling  $\Gamma_S$ , we have recorded full  $I$ - $V$  spectra on strained S-contacts. For reference, a spectrum of the normal, relaxed S-contact is displayed in Fig. 3b; the green tunnelling spectrum, recorded at the lateral position of a carboxylic oxygen atom (type A molecule), shows the well-known former LUMO of free PTCDA (P1), which in herringbone layers always appears at  $\varepsilon_0 = -0.15$  eV or  $-0.31$  eV (type A / type B) binding energy<sup>17</sup> (in fact, the spectrum in Fig. 3b shows a superposition of type A and type B levels, because the tip is located in the middle between the two); this resonance is a property of the molecules and their S-contacts and essentially independent of the type of T-contact (tunnelling or covalent). The width of P1 is determined by the substrate (or lead) coupling  $\Gamma_S$ . The figure indicates that, following the language of the Anderson Hamiltonian<sup>24</sup>, the relaxed S-contact is in the mixed valence regime  $\Gamma_S \geq \varepsilon_0$  (ref. 2), where transport electrons can hop on and off the molecule.

A completely different picture emerges if  $I$ - $V$  spectra are measured with the strained S-contact (Fig. 3c): Instead of P1 a very sharp and intense conductance peak directly at zero bias is observed. We propose this peak to be a Kondo resonance.

Sometimes, the T-contact is broken during the voltage ramp (possibly due to inelastic transport events), and only a part of the conductance peak is recorded. However, in almost all cases when the contact survives the voltage ramp, a clear Kondo peak as in Fig. 3c is observed. Altogether, we have recorded 15 complete Kondo peaks and many more incomplete ones. The Kondo effect arises if a local state (here: the molecular hybrid P1) with a twofold degeneracy interacts with delocalised electrons (here: electrons in the leads) having the same degeneracy<sup>10,24</sup>. Below the so-called Kondo temperature  $T_K$  the delocalised electrons screen the local state completely. In equilibrium, i.e. without a bias voltage, the density of states of the Kondo system below  $T_K$  must exhibit a sharp peak at the common Fermi level<sup>24</sup> – the Kondo resonance (Fig. 1c). Out of equilibrium, i.e. with a bias turned on, correlated tunnelling events of electrons into and out of the molecule (Fig. 1d) present a highly efficient transport channel which increases the initial differential conductance of the wire, yielding the Kondo resonance at  $V = 0$  in  $dI/dV$ -curves<sup>1-3</sup>. Coming back to the retraction curves in Fig. 3a, which have been recorded with a very low bias (2 mV), it is clear that the Kondo resonance, and thus many body correlations in the local orbital of the molecule, are responsible for the strong rise of the initial conductance – in Fig. 3a we essentially map out the intensity of the Kondo peak.

The peak in Fig. 3c is much sharper than the other relevant energy scales of the problem (see Fig. 1c for their definition):  $\varepsilon_0$  (binding energy of the local level),  $T_S$ , and  $U$  (correlation energy  $U$ , i.e. the energy necessary to overcome the Coulomb repulsion between two electrons in the local orbital). This is a hallmark of the Kondo resonance. From its FWHM of  $\Delta = 20$  mV a Kondo temperature of  $T_K \approx e\Delta / k_B = 240$  K can be estimated. We note that this Kondo temperature is much larger than  $T_K$  usually observed in single electron transistors ( $< 1$  K, refs. 3, 4), carbon nanotubes ( $< 10$  K, refs. 5, 6) or single atoms with molecular spacers (up to few tens of K, refs. 7, 8). This is similar to the findings of ref. 9 and reflects the very good covalent coupling of PTCDA to the

substrate<sup>14-17</sup>, even for the strained S-contact. The Kondo resonance should in principle be destroyed by thermal incoherence for temperatures larger than  $T_K$  (ref. 24). In the present case, this would require experiments at  $\approx 100$  K and above, which have turned out impossible because thermal drift prevents the stabilization of the covalent PTCDA junction.

Depending on the nature of the degeneracy, one differentiates between spin and orbital Kondo effects<sup>25</sup>. In the present case, orbital degeneracy is not expected<sup>17</sup>, so we assign the Kondo effect to the electron spin. In earlier STM work on the Kondo effect of isolated magnetic impurities on metal surfaces<sup>26,27</sup>, a Fano-type antiresonance was observed instead of the resonance in Fig. 3c; this was explained by destructive interference between two transport channels, one from the tip into the local level, the other into the delocalised states<sup>26,27</sup>. In the present case, such interference is not expected, because the covalent T-contact channels all transport electrons directly into the molecule. Therefore, we observe the “bare” Kondo resonance with its natural Lorentzian line shape.

The physical mechanism of  $\Gamma_S$ -tuning is the de-hybridisation of the molecular orbital P1 from the metal states. If we assume that the structural relaxation of the T-contact is small, the maximum in Fig. 3a corresponds to a  $\sim 5^\circ$  average tilt of the PTCDA molecule against the Ag surface (green curve in Fig. 2e) or an increase in the average molecule-metal distance of  $0.7 \text{ \AA}$ . We note that on this length scale a sizeable reduction of the hybridisation is indeed expected: On Au(111), the PTCDA-substrate distance is  $0.41 \text{ \AA}$  larger than on Ag(111) (Henze *et al.* to be published), and the molecule-substrate interaction is indeed much smaller. The de-hybridisation will increase the correlation energy  $U$ , because of better confinement of the local level to the molecule<sup>3,4</sup>, and decrease  $\Gamma_S$ , because of less metal-molecule wave function overlap. In the Anderson model<sup>24</sup> the ratio  $U/\Gamma$  controls whether the system is in the magnetic

(unpaired spin) or non-magnetic limit. Large  $U/\Gamma$  pushes the system into the limit of single occupancy (unpaired spin), also establishing the correlated Kondo spin-flip tunnelling channel by enforcing correlated movement in and out of the molecule. In this way, the Kondo effect can be observed although neither free nor chemisorbed PTCDA are magnetic.

We have also approached the Kondo regime from the weak coupling limit, by approaching a PTCDA molecule suspended from the tip to the silver surface. Again, we observe signatures of Kondo behaviour in the intermediate regime. The data are shown in the Supplementary Information c. Finally, the concept of the Kondo effect as a function of changing hybridisation at the PTCDA/Ag(111) interface is confirmed by the observation of a Kondo resonance for molecules with a naturally modified sample contact (Supplementary Information d).

It has been pointed out before that nanoelectronic devices offer the opportunity to create tunable model systems for transport experiments<sup>10</sup>, by choosing suitable voltages, magnetic fields etc. in single electron transistor<sup>2-4</sup> or carbon nanotube<sup>5,6</sup> devices, or by using molecular tethers of well-adjusted length<sup>8</sup>. In the present case, the detailed, atomic-level structure of a molecule/metal contact has been manipulated, thereby tuning the hybridisation between a single molecule and its substrate. The experiments reported here have been carried out on the  $\pi$ -metal contact which is an important element of organic and molecular electronics<sup>28</sup>. We anticipate that our results will allow detailed comparison with transport and chemisorption theory at the *ab initio* level<sup>29</sup>. On a more general note the approach taken here may be a new pathway to well-defined single molecule experiments. In particular, our experiments combine efforts to symmetrize the STM junction<sup>19,20</sup> and thus increase its relevance for transport experiments with optimal contact control by using molecules from epitaxial layers.



**Acknowledgements:** The work was financially supported by the Deutsche Forschungsgemeinschaft (DFG). The authors are grateful to G. Cuniberti and B. Song (Universität Regensburg, Germany) for helpful discussions.

## Methods

**Height calibration.** Experiments have been carried out in a low temperature STM (Createc GmbH) in ultra high vacuum at 10 K. The calibration of the STM piezoelectric scanner was tested by measuring the height of a mono-atomic Ag(111) step. The result of  $2.433 \text{ \AA}$  is in very good agreement with the expected value of  $2.356 \text{ \AA}$ . In all approach and retraction curves of this letter the  $z$ -coordinate along the abscissa quantifies the distance of the tip from the average position of the PTCDA carboxylic oxygen atoms. This scale has been calibrated in the following way. (1) The tip is stabilized at  $I = 0.1 \text{ nA}$  and  $V_b = -340 \text{ mV}$  (“stabilisation point”) above the maximum of the PTCDA P1 state. (2) With closed feedback loop, the tip is moved above bare Ag, whence the tip moves  $(0.75 \pm 0.02) \text{ \AA}$  toward to the surface. (3) The feedback loop is opened and the tip is moved into contact with the Ag surface. After appropriate correction<sup>30</sup>, the corresponding  $z$ -piezo shift yields an absolute tip height above Ag. From this absolute calibration and the knowledge of the adsorption height of carboxylic oxygen above PTCDA<sup>15</sup>, a tip height of  $(6.7 \pm 1.6) \text{ \AA}$  above the carboxylic oxygens of PTCDA at the stabilisation point is calculated. The uncertainty of  $1.6 \text{ \AA}$  originates from considering two extreme (and unlikely) limits of tip-surface contacts. In reality, the (statistical) error bar will be much smaller; we estimate an error of  $\pm 0.8 \text{ \AA}$ . A typical approach curve with the definition of the tip-metal contact point and a schematic of the complete  $z$ -calibration process are shown in the Supplementary Figure 1b and discussed there.

## References

- [1] Meir, Y., Wingreen, N.S. & Lee, P.A. Low temperature transport through a quantum dot: The Anderson model out of equilibrium. *Phys. Rev. Lett.* **70**, 2601-2605 (1993).
- [2] Goldhaber-Gordon, D. et al. From the Kondo regime to the mixed valence regime in a single electron transistor. *Phys. Rev. Lett.* **81**, 5225-5228 (1998).
- [3] Cronenwett, S.M., Oosterkamp, T.H. & Kouwenhoven, L.P. A tunable Kondo effect in quantum dots. *Science* **281**, 540-544 (1998).
- [4] Goldhaber-Gordon, D. et al. Kondo effect in a single-electron transistor. *Nature* **391**, 156-159 (1998).
- [5] Nygard, J., Cobden, D.H. & Lindelof, P.E. Kondo physics in carbon nanotubes. *Nature* **408**, 342-346 (2000).
- [6] Jarillo-Herrero, P. et al. Orbital Kondo effect in carbon nanotubes. *Nature* **434**, 484-488 (2005).
- [7] Liang, W., Shores, M.P., Bockradt, M., Jong, J.R., & Park, H. Kondo resonance in a single-molecule transistor. *Nature* **417**, 725-729 (2002).
- [8] Park, J. et al. Coulomb blockade and the Kondo effect in single-atom transistors. *Nature* **417**, 722-725 (2002).
- [9] Zhao, A., et al. Controlling the Kondo effect of an adsorbed magnetic ion through its chemical bonding. *Science* **309**, 1542-1544 (2005).
- [10] Potok, R. M. & Goldhaber-Gordon, D. New spin on correlated electrons. *Nature* **434**, 451-452 (2005).
- [11] Cuniberti, G., Fagas, G. & Richter, K. (Eds.) *Introducing Molecular Electronics*. Lecture Notes in Physics , Vol. 680 (Springer, Berlin, 2005)

- [12] A. Nitzan & M. A. Ratner. Electron transport in molecular wire junctions. *Science* **300**, 1384-1389 (2003).
- [13] Glöckler, K. et al. Highly ordered structures and submolecular scanning tunneling microscopy contrast of PTCDA and DM-PBDCI monolayers on Ag(111) and Ag(110). *Surf. Sci.* **405**, 1-20 (1998).
- [14] Eremtchenko, M., Schaefer, J.A. & Tautz, F.S. Understanding and tuning the epitaxy of large aromatic adsorbates by molecular design. *Nature* **425**, 602-605 (2003).
- [15] Hauschild, A. et al. Molecular distortions and chemical bonding of a large  $\pi$ -conjugated molecule on a metal surface. *Phys. Rev. Lett.* **94**, 036106(4) (2005).
- [16] Zou, Y. et al. Chemical bonding of PTCDA on Ag surfaces and the formation of interface states. *Surf. Sci.* **600**, 1240-1251 (2006).
- [17] Kraft, A. et al. Lateral adsorption geometry and site-specific electronic structure of a large organic chemisorbate on a metal surface. *Phys. Rev. B* **74**, 041402(R) (2006).
- [18] Temirov, R., Soubatch, S., Luican, A., & Tautz, F.S. Free-electron-like dispersion in an organic monolayer film on a metal substrate. *Nature* in press (2006).
- [19] Li, Z., Han, B., Meszaros, G., Pobelov, I., Wandlowski, Th., Blaszczyk, A. & Mayor, M. Two-dimensional assembly and local redox-activity of molecular hybrid structures in an electrochemical environment. *Faraday Discussions* **131**, 121-143 (2006).
- [20] Neel, N. et al. Controlled Contact to a C<sub>60</sub> Molecule. cond-mat/0608476.
- [21] Naydenov, B., Ryan, P., Teague L.C. and Boland, J. J. Measuring the Force of Interaction between a Metallic Probe and a Single Molecule. *Phys. Rev. Lett.* **97**, 098304(4) (2006).
- [22] Darr, J.A., Poliakoff, M., Li, W.S. and Blake, A.J. Hexafluoropentanedionato-silver(I) complexes stabilised by multidentate N-donor ligands: crystal structure of a

- charge-separated salt species soluble in supercritical carbon dioxide. *J. Chem. Soc., Dalton Trans.*, 2869 - 2874 (1997) .
- [23] Albrecht, M., Schnurpfeil, A, & Cuniberti, G. From a local Green's function to molecular charge transport. *Phys. Stat. Sol. (b)* **241**, 2179-2188 (2004).
- [24] Hewson, A.C. *The Kondo Problem to Heavy Fermions* (Cambridge. Univ. Press, Cambridge, 1993).
- [25] Cox, D.L. & Zawadowski, A. Exotic Kondo effects in metals: magnetic ions in a crystalline electric field and tunnelling centres. *Adv. Phys.* **47**, 599-942 (1998).
- [26] Li, J., Schneider, W.D., Berndt, R. & Delley, B. Kondo scattering observed at a single magnetic impurity. *Phys. Rev. Lett.* **80**, 2893-2896 (1998)
- [27] Madhavan, V., Chen, W., Jamneala, T., Crommie, M.F. & Wingreen, N.S. Tunneling into a single magnetic atom: Spectroscopic evidence of the Kondo resonance. *Science* **280**, 567-569 (1998).
- [28] Cahen, D., Kahn, A. & Umbach, E. Energetics of molecular interfaces. *Mater. Today* **8**, 32-41 (2005).
- [29] Nemeč, N., Tomanek, D., & Cuniberti, G. Contact dependence of carrier injection in carbon nanotubes: An ab initio study. *Phys. Rev. Lett.* **96**, 076802(4) (2006).
- [30] Hofer, W.A., Fisher, A.J., Wolkow, R.A. & Grütter, P. Surface relaxations, current enhancements, and absolute distances in high resolution scanning tunnelling microscopy. *Phys. Rev. Lett.* **87**, 236104(4) (2001).

**Figure 1 | Single molecule transport experiment on PTCDA/Ag(111).** **a**, chemical formula and side view of PTCDA bonding to Ag(111), with (i) primary bond via the LUMO and (ii) secondary bond via the carboxylic oxygen atoms (vertical distortion is shown schematically). For clarity the lobes of the LUMO at the carboxylic oxygen atoms have been left out. Yellow arrows: Charge transfer from metal to LUMO due to primary bond. Covalent contacts to the molecule are shown by blue line (point-like T-contact) and blue rectangle (extended S-contact). Electron transport through molecular wire is shown by red arrow. **b**, schematic of strained S-contact due to tip retraction. At the maximum of the conductance in Fig. 3a the tilt corresponds to the  $5^\circ$  shown in the image, assuming for simplicity that the molecule does not buckle (in reality, buckling is likely). On the left a schematic of the molecular wire is shown, with the two lead coupling constants  $\Gamma_T$  and  $\Gamma_S$ . **c**, schematic density of states of a molecule between two contacts in equilibrium ( $V_b=0$ ).  $\epsilon_0$ ,  $U$ , and  $I = \Gamma_T + \Gamma_S$  are the parameters of the Anderson model<sup>24</sup>. Black: density of states for  $T \gg T_K$ . For  $T < T_K$ , the Kondo resonance (red) arises additionally. **d**, the molecular wire under bias  $V_b = \mu_T - \mu_S$ , where  $\mu$  are the chemical potentials in the leads, with a correlated tunnelling event due to the Kondo effect: Black (red) arrows indicate electron spins before (after) the event. Thin arrows indicate the electron tunnelling.

**Figure 2 | Forming a covalent contact between the STM tip and PTCDA.** **a**, STM image of herringbone phase of PTCDA on Ag(111). ( $5 \times 5 \text{ nm}^2$ ,  $I = 0.16 \text{ nA}$ ,  $V_b = -340 \text{ mV}$ ). Molecules of type A and B are marked. Inset: Vacancy island created by removing PTCDA molecules with the tip. Image  $10 \times 7 \text{ nm}^2$ ,  $I = 0.1 \text{ nA}$ ,  $V_b = -340 \text{ mV}$ . **b**, STM image as in a, but  $I = 3 \text{ nA}$ ,  $V_b = -15 \text{ mV}$ , corresponding to a distance of  $(2.4 \pm 0.8) \text{ \AA}$  above the carboxylic oxygens. **c**, approach spectrum recorded above a carboxylic oxygen with  $V_b = -2 \text{ mV}$ .

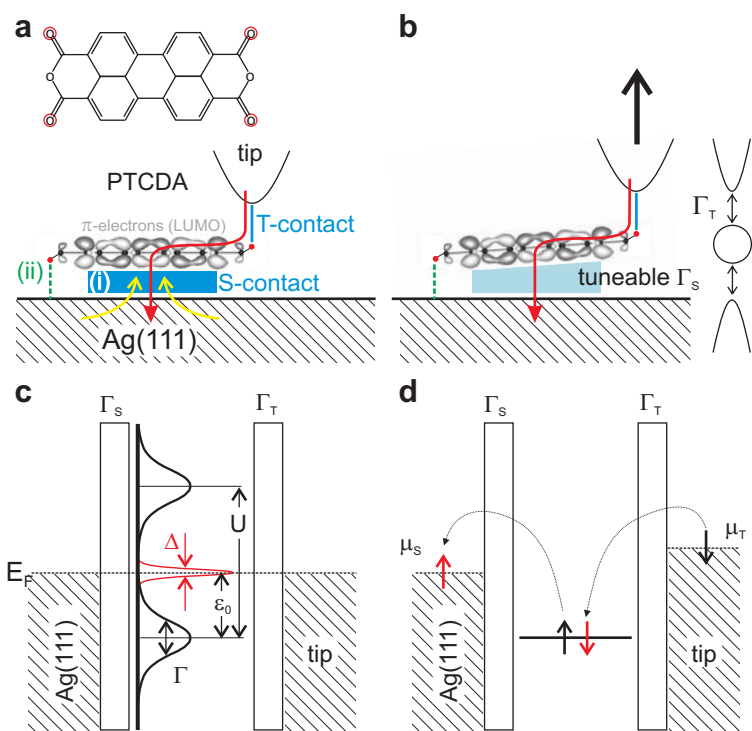
Conductance in units of  $G_0 = 2e^2/h = (12.9 \text{ k}\Omega)^{-1}$ . Interpretation of the two conductance jumps in the inset. For all z-calibrations in this Figure, cf. Methods. **d**, curves 1 and 2: Distribution of conductances, evaluated on dataset consisting of 282 approach curves like in c, all carried out with identical tip. Curves 1 (wine) and 2 (magenta) – conductances in the tunnelling regime before the flip, corresponding to point 1 in c, and immediately after the flip, corresponding to point 2 in c, respectively. Green curve – distribution of conductance maxima occurring for the strained S-contact, cf. Fig. 3a, based on 146 retraction curves. **e**, distribution of tip-to-carboxylic-oxygen distances at which the flip occurs; red – aligned PTCDA (type A), blue – misaligned PTCDA (type B). Data (recorded with several different tips) are based on 110 approaches for type A and 115 approaches for type B. Green curve: distribution of tip-to-carboxylic-oxygen distances at which conductance maximum (as in Fig. 3a) occurs.

### **Figure 3 | Transport properties with relaxed and strained S-contact:**

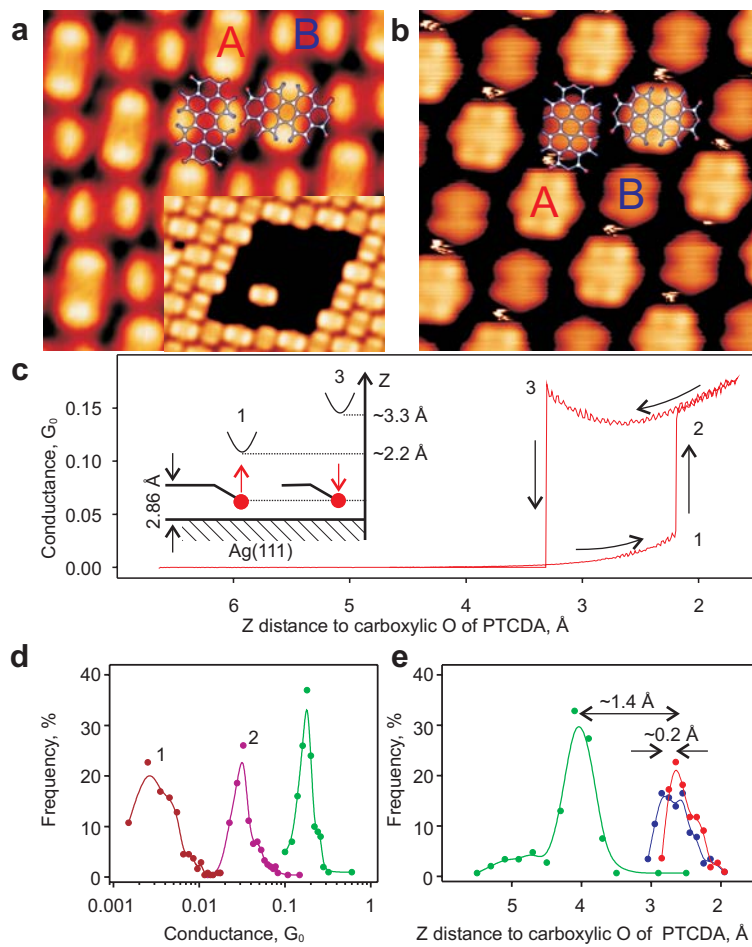
**Kondo effect.** **a**, collection of 282 retraction spectra recorded with identical tip (same dataset as in Fig. 2d). Brightness scales with frequency of events. inset: Typical approach and retraction cycle without breaking of the T-contact,  $V_b = 2$  mV. For all z-calibrations in this Figure, cf. Methods. **b**, differential conductance  $dI/dV_b$  (green curve, left scale) and  $I-V_b$  characteristics (black curve, right scale) recorded at a distance of  $z = (3.7 \pm 0.8) \text{ \AA}$ , i.e. in the tunnelling regime before the flip, above carboxylic oxygen atom. Parameters: modulation amplitude  $V_{\text{mod}} = 4$  mV, modulation frequency  $\nu_{\text{mod}} = 1305.3$  Hz, recording time 120 sec. Red (blue) curves are tunnelling spectra (arbitrary intensity) recorded above the maximum of P1 for type A (type B) molecules, taken from ref. 18. Parameters from Anderson Hamiltonian are indicated. Dashed curve is taken from Fig. 3c. **c**, differential conductance  $dI/dV_b$  (green, left scale) and  $I-V_b$  characteristics (black, right scale) recorded for a strained S-contact at a distance of  $z = (5.2 \pm$

0.8) Å, i.e. after T-contact formation and during pulling. Parameters: modulation amplitude  $V_{\text{mod}} = 4$  mV, modulation frequency  $\nu_{\text{mod}} = 1305.3$  Hz, recording time 100 sec.

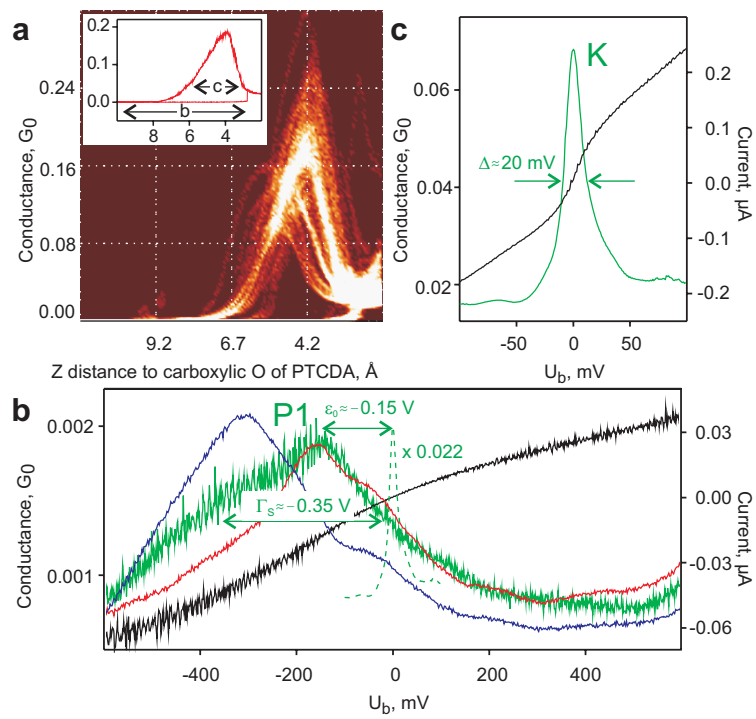




Temirov & Tautz (2006), Figure 1



Temirov & Tautz (2006), Figure 2

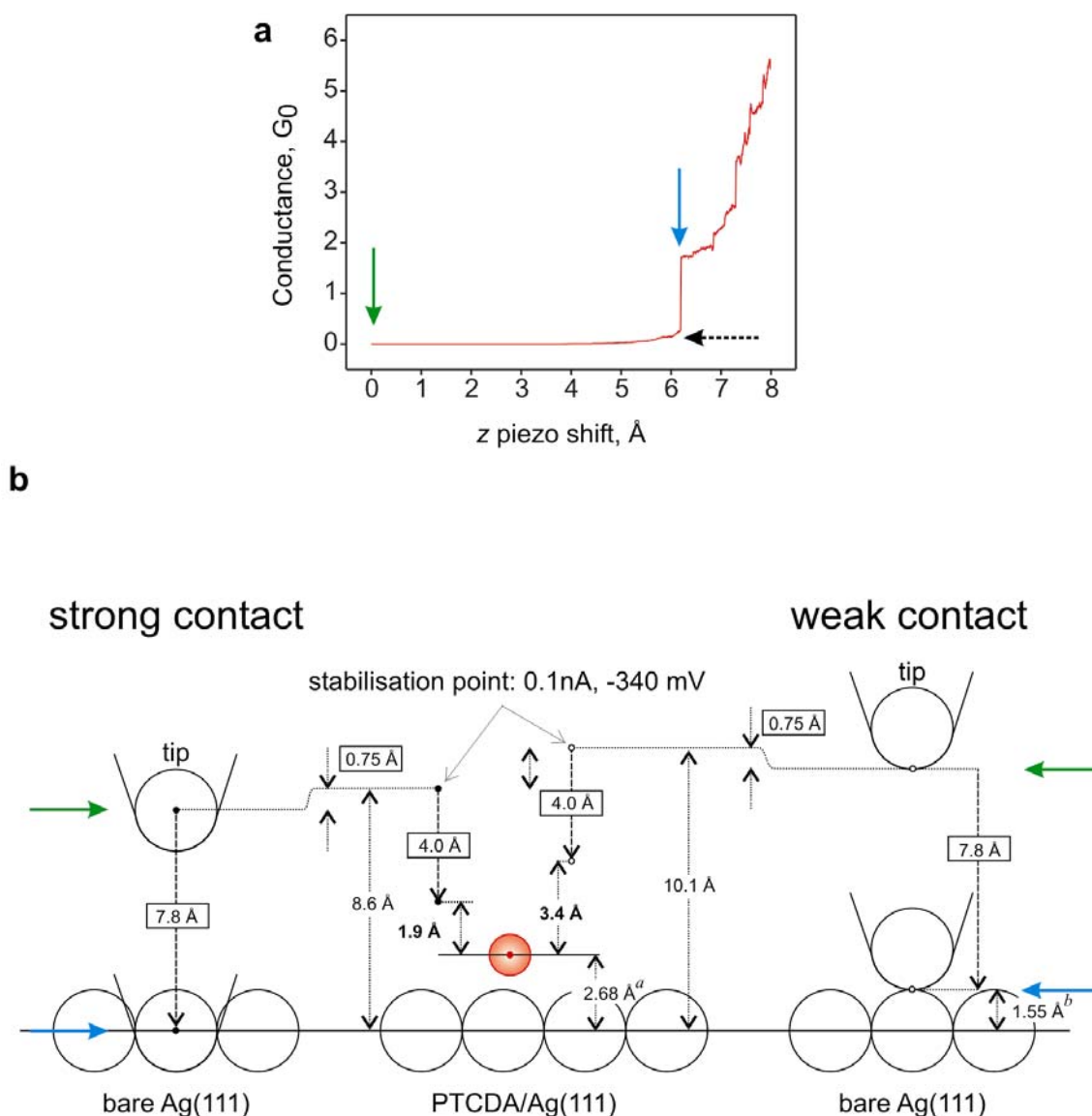


Temirov & Tautz (2006), Figure 3

## Supplementary Information

### (a) Carboxylic oxygen atoms flip up on contact formation

In the main paper, we have stated that the 0.2 Å offset in the response of the carboxylic oxygen atoms on the two types of molecules (Fig. 2e) proves that the oxygen atoms move toward the tip, rather than the apex atom of the tip toward the oxygen atom. This follows from the fact that the height difference between the carboxylic oxygen atoms on the two molecules is of the order 0.05 to 0.1 Å and hence considerably less than 0.2 Å (M. Rohlfing, private communication). We can thus conclude that the flip occurs for shorter tip-oxygen distances on A-molecules than B-molecules. This strongly suggests that the A-oxygen atom is stronger bonded and hence needs a larger force (i.e. closer tip) to separate it from the substrate. In fact, it is known from *ab initio* calculations that the A-type molecule is bonded stronger than the B-type molecule. On the other hand, the large number of experiments in Fig. 2e excludes a systematic difference of the bonding of the tip apex atom in experiments on A- and B-molecules. Alternatively, one could speculate that the interaction force between the tip apex and the carboxylic oxygen is systematically lower for A-type molecules than B-type molecules, leading to a delayed flip of the tip apex atom in the former case; this, however, seems very unlikely. We thus finally conclude that it must be the carboxylic oxygen atoms which move up, as shown schematically in Fig. 1a/b and the inset to Fig. 2c.



**Supplementary Figure 1 | Approach spectrum above Ag(111) and  $z$ -calibration.** **a**, Approach spectrum measured with a bias of  $V_b = -2$  mV. Before opening the feedback loop, the tip was stabilised at  $I = 0.1$  nA and  $V_b = -340$  mV. Dashed arrow indicates the total distortion of the tip-sample contact. Blue and green arrows correspond to the position marked in **b**. **b**, Scale model of the  $z$ -calibration procedure. Left and right panels: Approach above Ag(111) (cf. Methods, step 3), assuming weak and strong contacts. Middle panel: Approach above carboxylic oxygen atoms, the latter represented by a red circle with covalent radius of  $r_c = 0.7$  Å (ref. 32). Tip and substrate atoms are represented by open circles with the covalent radius of silver ( $r_c = 1.55$  Å) (ref. 32). Framed distances are piezo-shifts. <sup>a</sup> The experimental value has been taken from ref. 15. <sup>b</sup> The value has been taken from ref. 32. Further discussion in the text of the Supplementary Information, section b.

### (b) Absolute $z$ -calibration of approach spectra

It is stated in the main paper that the Ag-O distance of the T-contact is  $(2.9 \pm 0.8)$  Å. It is clear that this value depends on an accurate calibration of the  $z$ -scale. The general

approach used in the present work is described in the Methods section. Here we provide the details of the calibration procedure.

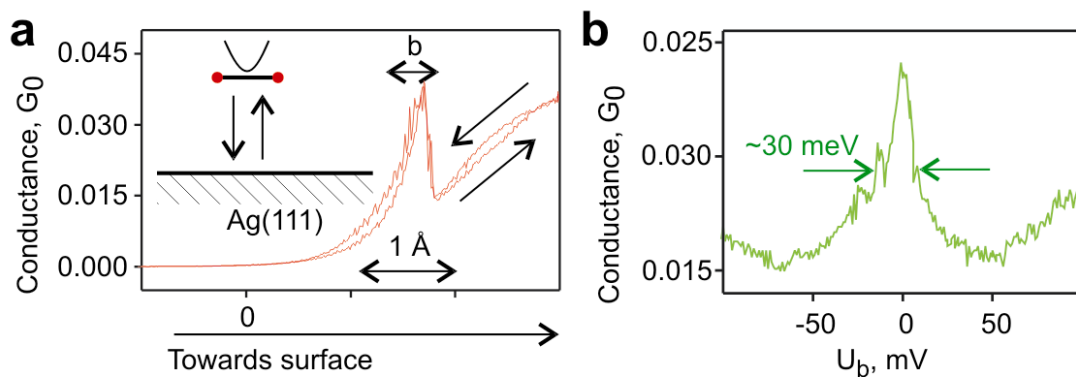
Once the tip has been placed above the Ag surface at  $I = 0.1$  nA,  $V_b = -340$  mV (completion of step 2, cf. Methods), it is moved towards the Ag surface until contact is made (step 3). A typical approach curve above Ag is shown in Supplementary Fig. 1a. The step at  $(6.3 \pm 0.2)$  Å indicates that contact has been made. In the present example, the conductance after the step is  $1.7 G_0$ . Values in this range, and in particular larger than  $G_0$ , are common for tip contacts with flat surfaces<sup>31</sup>. This proves that more than one conduction channel has been established, indicating in turn that the contact is not formed between just the single apex atom and a single atom in the surface.

The contact appears after a piezo-shift of  $(6.3 \pm 0.2)$  Å (Supplementary Fig. 1a). This value, however, must be corrected, because the attractive forces between tip and surface distort both of them before the contact is made. This distortion has been calculated quantitatively in ref. 30, with the result that the tip and sample move towards each other by 1 to 2 Å; contact is hence made at a value on the piezo-scale for which the undistorted tip would still be 1 to 2 Å away from the undistorted surface. When seeking to determine the distance of a tip to the lattice planes of a surface, in the regime when the tip is far away from the surface and therefore both are undistorted, we therefore have to add 1 to 2 Å to the piezo-shift determined from an approach curve such as presented in Supplementary Fig. 1a. The tip-to-sample distance in Supplementary Fig. 1b is therefore  $(6.3 + 1.5 \pm 0.5)$  Å =  $(7.8 \pm 0.5)$  Å. Having accounted for the distortion effect by the  $(+1.5 \pm 0.5)$  Å correction, we can from now on disregard the distortion of tip and sample in our discussion.

The next issue is the atomic structure of the contact at the point of the conductance jump in Supplementary Fig. 1a. In Supplementary Fig. 1b we consider two

limits: On the right, a weak contact is shown, assuming that the current jump occurs when the apex atom goes into first mechanical contact with the surface. On the left, the strong contact supposes that the apex atom becomes completely embedded in the first atomic layer of the surface. These contacts are extreme limits. Reality will lie somewhere in between. The conductance value of  $1.7 G_0$  indicates that the contact must be stronger than the weak contact on right of Supplementary Fig. 1b. In the following, we will base our calculations on both scenarios and interpolate between them. According to the Figure, they lead to an absolute tip height above Ag at the stabilisation point of  $(9.4 \pm 1.6) \text{ \AA}$ . This corresponds to  $(6.7 \pm 1.6) \text{ \AA}$  above the carboxylic oxygen atoms. The uncertainty of  $1.6 \text{ \AA}$  originates from considering two extreme (and unlikely) limits of tip-surface contacts.

In the middle panel of Supplementary Fig. 1b the approach towards the carboxylic oxygen (displayed in red) is shown schematically. The piezo-shift to the point on the piezo-scale where the flip occurs is  $4.0 \text{ \AA}$  (cf. Fig. 2e), yielding  $1.9$  or  $5.0 \text{ \AA}$  [=  $(3.4 \pm 1.6) \text{ \AA}$ ] as the centre-to-centre distance of the tip apex atom to the carboxylic oxygen just before the flip. From the distortion of the molecule (the carboxylic oxygen is  $0.2 \text{ \AA}$  below the average carbon position) we estimate an oxygen movement by  $\sim 0.5 \text{ \AA}$  to a symmetric position above the plane of the molecule. This yields an estimated Ag-O bonding distance of  $(2.9 \pm 1.6) \text{ \AA}$ . The uncertainty in this number is given by the two limits of a strong and weak tip-Ag contact during  $z$ -calibration; the most likely value, corresponding to an ‘intermediate’ tip-Ag contact is indeed the central value of  $2.9 \text{ \AA}$ . In reality, the (statistical) error bar will be much smaller; we estimate an error of  $\pm 0.8 \text{ \AA}$  for the range of realistic tip-metal contacts. The Ag-O bond distance of  $(2.9 \pm 0.8) \text{ \AA}$  is in reasonable agreement with known distances of Ag-O bonds (cf. main paper).



**Supplementary Figure 2 | Observation of the Kondo effect on approaching the PTCDA molecule to the substrate.** **a**, Approach spectrum towards the bare Ag(111) surface with a PTCDA molecule on the tip apex,  $V_b = -100$  mV, recording time 5 sec. Tip stabilized at  $I = 0.52$  nA,  $V_b = -22$  mV before opening of the feedback loop, peak maximum reached at  $\Delta z \approx +1.7$  Å. **b**, differential conductance  $dI/dV_b$  recorded at  $\Delta z \approx +2.5$  Å after approaching the bare Ag(111) surface with a PTCDA molecule on the tip. Parameters: modulation amplitude  $V_{\text{mod}} = 4$  mV, modulation frequency  $\nu_{\text{mod}} = 743.3$  Hz, recording time 100 sec.

### (c) Observation of Kondo effect on approaching the molecule to the substrate

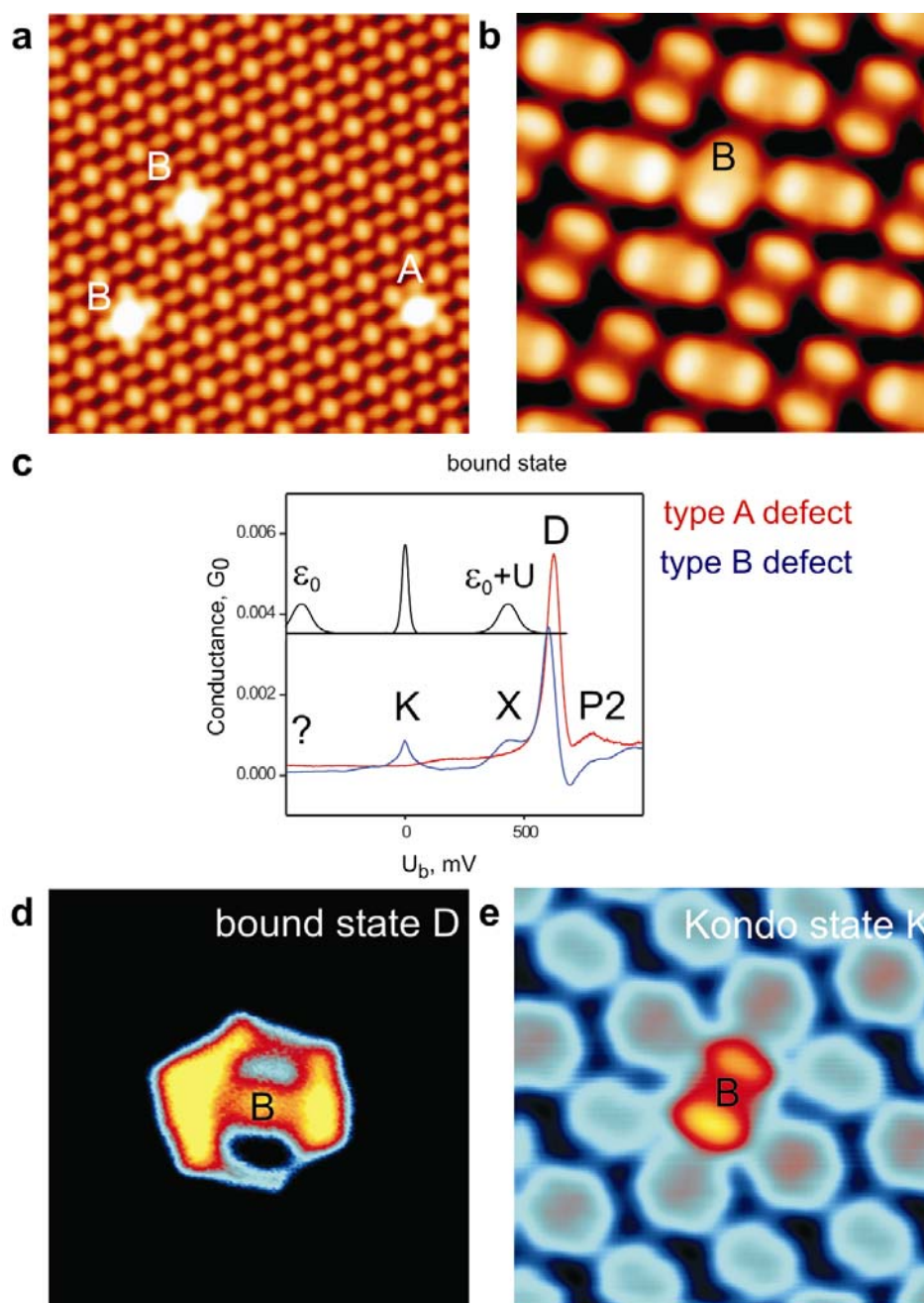
In the main paper we sample a Kondo resonance by starting in the mixed-valence regime and reducing the lead coupling into the intermediate regime by controlled bond cleavage. In principle, it should also be possible to enter the same intermediate coupling regime from the weak coupling side, i.e. by approaching a tip-suspended molecule together with the tip towards the metal surface.

As Supplementary Figs. 2a and 2b show, this is indeed possible. Supplementary Fig. 2a displays an approach and retraction curve of a tip with a molecule attached to it. The molecule has been picked up with the tip in the same way as described in the context of the inset of Fig. 2a in the main paper. On approaching the sample with this tip, we once more observe a clear maximum in the initial conductance, qualitatively similar in Fig. 3a of the main paper. If a full  $I$ - $V$  curve is measured in the distance regime where this maximum appears, we again observe a Kondo resonance, of similar width as before (Supplementary Fig. 2b).



Two differences to the cleaving experiments are striking: First, the peak in the conductance occurs on a significantly shorter length scale (i.e. is much sharper in the z-position coordinate), and secondly, there is very little hysteresis between the approach and retraction half-cycles in Supplementary Fig. 2a. Both these observations can be naturally explained by assuming that the molecule is bonded centrally and therefore much more rigidly to the tip (as shown schematically in the inset of Supplementary Fig.2a), preventing the possibility to tilt or bend the molecule on approach and retraction. It is clear that after the removal of a molecule from the Ag(111) sample we lose control over the structure of the tip-molecule complex, because the molecule can move into a new bonding configuration after the S-contact has been severed. According to what we know about the bonding of PTCDA on metal surfaces (in most cases flat via the  $\pi$ -metal interaction), it is therefore quite likely that the molecule bonds centrally to the tip eventually. From the imaging behaviour as well as from approach curves in Supplementary Fig. 2a it is very clear, however, that we still have a PTCDA molecule present in the tunnelling region of the tip. Freshly prepared tips never exhibit the behaviour displayed in Supplementary Figs. 2a and 2b.

Finally, we note that the relevant length scale in Supplementary Fig. 2a (approximately 1 Å) is still wide enough for tuning the hybridisation from negligible to sufficiently strong to observe a Kondo effect. The rise on the left hand side of the graph is most likely due to the improved contact formation in a regime where the tip presses against the sample.



**Supplementary Figure 3 | Observation of the Kondo effect for a molecule with a naturally modified sample contact.** **a**, STM image ( $20 \times 20 \text{ nm}^2$ ,  $I = 0.1 \text{ nA}$ ,  $V_b = 500 \text{ mV}$ ) of the PTCDA/Ag(111) herringbone phase with 3 defect molecules on sites as labelled. **b**,  $5 \times 5 \text{ nm}^2$  zoom of a B-type defect molecule from **a**,  $I = 0.1 \text{ nA}$ ,  $V_b = -340 \text{ mV}$ . **c**, STS spectra measured at the position of the LUMO lobe of B-type defect (blue, recording time 480 sec) and A-type defect (red, recording time 240 sec). Tip stabilized at  $I = 0.51 \text{ nA}$ ,  $V_b = -340 \text{ mV}$ . Modulation amplitude  $V_{\text{mod}} = 4 \text{ mV}$ , modulation frequency  $\nu_{\text{mod}} = 1233.3 \text{ Hz}$  (blue) and  $\nu_{\text{mod}} = 1333.3 \text{ Hz}$  (red). **d**, STS image ( $5 \times 5 \text{ nm}^2$ ) of the bound state D at a B-type defect molecule,  $I = 0.51 \text{ nA}$ ,  $V_b = 625 \text{ mV}$ , modulation amplitude  $V_{\text{mod}} = 4 \text{ mV}$ , modulation frequency  $\nu_{\text{mod}} = 1333.3 \text{ Hz}$ . **e**, STM image ( $5 \times 5 \text{ nm}^2$ ) of the Kondo state K at a B-type defect molecule,  $I = 0.52 \text{ nA}$ ,  $V_b = 40 \text{ mV}$ .

#### **(d) Observation of a Kondo resonance for a molecule with a naturally modified sample contact**

In the main paper we explain the approach curves in Fig. 3a and the sharp resonance feature in Fig. 3c by the Kondo effect which occurs as the S-contact of the molecule is gradually cleaved. Further proof that the observed transient behaviour of the conductance is generated at the S-contact, and not an artefact of the stretching experiment or even related the T-contact, comes from the observation of Kondo behaviour at the PTCDA/Ag(111) interface in the conventional tunnelling regime for molecules with a naturally modified sample contact, namely at certain defect molecules in the herringbone layer.

Supplementary Fig. 3a shows a large scale image of a PTCDA herringbone layer. The three bright objects correspond to molecules which are bonded differently to the Ag(111) surface than the standard molecules. Their extreme brightness originates from a bound state (labelled D, Supplementary Fig. 3c) which splits off from the bottom of the delocalised P2-state<sup>18</sup> in herringbone layers due to strong local scattering. Such defects are always observed in room temperature-prepared PTCDA monolayers at both A and B sites. The exact nature of the defect is not known. Very likely, they are PTCDA molecules, as high resolution images suggest (Supplementary Fig. 3b); the origin of their different electronic properties could be an Ag vacancy or adatom below the molecule, or some other co-adsorbate. However, it is not possible to exclude a small chemical variation of the PTCDA molecule\*.

The important point here is that a slight change of the hybridisation with the substrate, whatever the origin, leads to a very strong change in the electronic structure

---

\* Unfortunately, it has not been possible to image either vacancy, adatom or coadsorbate after taking away a defect molecule by tip manipulation.

of the molecule: As Supplementary Fig. 3c shows, defect molecules show the same type of Kondo behaviour as the strained S-contact. This proves that reducing the hybridisation at the metal-molecule bond in this system really has the potential to induce Kondo behaviour. Remarkably, we observe a very strict difference between defect molecules at aligned (A) and misaligned (B) sites: Only defects at B sites exhibit Kondo behaviour, while the aligned defect shows a broad peak above the Fermi level which may be the unfilled LUMO. Note also that the X-state always appears together with the Kondo peak. While K is always constant in energy, X is shifting a little from defect to defect. One may speculate that this peak is related to the  $\varepsilon_0+U$  peak in the spectral function of the Anderson model<sup>24</sup>. Unfortunately, we never see the peak  $\varepsilon_0$  on the occupied side, which may be coupled to general problems with spectroscopy in this bias regime at the PTCDA/Ag(111) interface<sup>17</sup>. We have checked for a correlation of the position of peak X with the Kondo temperature as determined from the width of the Kondo resonance, but if at all, we only find a very weak one.

[31] Limot, L., Kröger, J., Berndt, R., Garcia-Lekue, A., & Hofer, W.A. Atom transfer and single-atom contacts. *Phys. Rev. Lett.* **94**, 126102(4) (2005).

[32] [www.webelements.com](http://www.webelements.com)